



ELSEVIER

Contents lists available at ScienceDirect

Ceramics International

journal homepage: www.elsevier.com/locate/ceramint

Balance of oxygen throughout the conversion of a high-level waste melter feed to glass

SeungMin Lee^{a,*}, Pavel Hрма^a, Jaroslav Kloužek^{b,c}, Richard Pokorný^{b,c}, Miroslava Hujová^{b,c}, Derek R. Dixon^a, Michael J. Schweiger^a, Albert A. Kruger^d

^a Pacific Northwest National Laboratory, Richland, WA 99352, USA

^b Laboratory of Inorganic Materials, Joint Workplace of the University of Chemistry and Technology Prague, Technická 5, 166 28 Prague 6, Czech Republic

^c The Institute of Rock Structure and Mechanics of the ASCR, v.v.i., V Holešovičkách 41, 182 09 Prague 8, Czech Republic

^d US Department of Energy, Office of River Protection, Richland, WA 99352, USA

ARTICLE INFO

Keywords:

Oxygen mass balance
Feed-to-glass conversion
Evolved gas
Oxygen partial pressure
Fe redox ratio

ABSTRACT

Gases evolve from nuclear waste melter feed during conversion to glass in response to heating. This paper is focused on oxygen mass balance based on the stoichiometry of feed melting reactions and evolved-gas analysis data. Whereas O₂-producing and -consuming batch-melting reactions are complete in the reacting and primary-foam layers of the cold cap, O₂ from redox reactions continues to evolve as long as melt temperature increases, and thus generates secondary foam. Also, we discuss the relationship between the oxygen mass balance and the temperature-dependent iron redox ratio and the O₂ partial pressure, as they evolve during the feed-to-glass conversion.

1. Introduction

Vitrification is an established method to immobilize nuclear waste. The waste is mixed with glass-forming and -modifying additives and charged into a melter. In a joule-heated melter into which the feed is charged as slurry, melter feed forms the cold cap that floats on molten glass [1,2]. The cold cap consists of two layers (Fig. 1): the reaction layer, from which gases are freely escaping through open pores [3–7], and the foam layer, in which gases are trapped. Pokorný et al. [8] and Chun et al. [9] analyzed the kinetics of gas-evolving feed reactions and Rodriguez et al. [5] identified the gases using evolved-gas analysis (EGA).

Residual gases are trapped in bubbles when the glass-forming melt becomes connected. As bubbles grow, the bubbly melt turns to primary foam that eventually collapses [1,10]. Unless foaming is extremely vigorous, primary foam bubbles descend with melt and merge into cavities that escape sideways. Bubbles also ascend from the glass melt to form secondary foam (Fig. 1). Secondary bubbles originate from multivalent oxides that release oxygen in response to increasing temperature and from sulfate that releases SO₂ and O₂.

Foam tends to insulate the reaction layer from heat incoming from molten glass below. Foam can be destabilized by promoting forced convection in the melt (usually by bubbling gas [11]) or decreasing melt viscosity via glass composition or higher temperature [12]. Since

the sources of gas are raw materials, modifying the feed makeup is another efficient way of affecting foaming.

In commercial glass batches, the raw materials are selected according to the cost, ease of melting, and efficient removal of bubbles [13]. For example, Na₂O is supplied as soda, but can also be added in the form of soda ash [14] or sodium sulfate [15]; SiO₂ is commonly introduced as silica sand or crushed quartz of a controlled grains-size [16–19]. Special additives are used for enhancing bubble removal, such as sulfate in combination with carbon or fining agents that change the redox state on heating (e.g., combination of sodium nitrate and antimony) [20].

Typically, about half of the waste glass mass originates from the waste. The rest are glass forming and modifying additives the mineral form of which can be chosen to maximize the rate of melting via their effect on the extent and the mode of foaming. Quartz (silica) grain size can vary between 1 μm and 1 mm [12,21]. Alkali and alkaline earth oxides can be introduced as nitrates or carbonates [22]. Feeds could contain reducing agents (e.g., sucrose [23] or oxalic acid [24]). Feed components can be calcined or pre-vitrified to frit [25,26]. Alumina can be added as boehmite [AlO(OH)], gibbsite [Al(OH)₃], corundum (Al₂O₃), nepheline (NaAlSiO₄), etc. [10,27,28]. In this study, we focus on the effect of the mineral source of Al₂O₃ on O₂ evolution that in turn influences the extent of foaming as the melter feed is converted to molten glass [10,27,28].

* Corresponding author.

E-mail address: seungmin.lee@pnnl.gov (S. Lee).

<http://dx.doi.org/10.1016/j.ceramint.2017.07.002>

0272-8842/ © 2017 Elsevier Ltd and Techna Group S.r.l. All rights reserved.

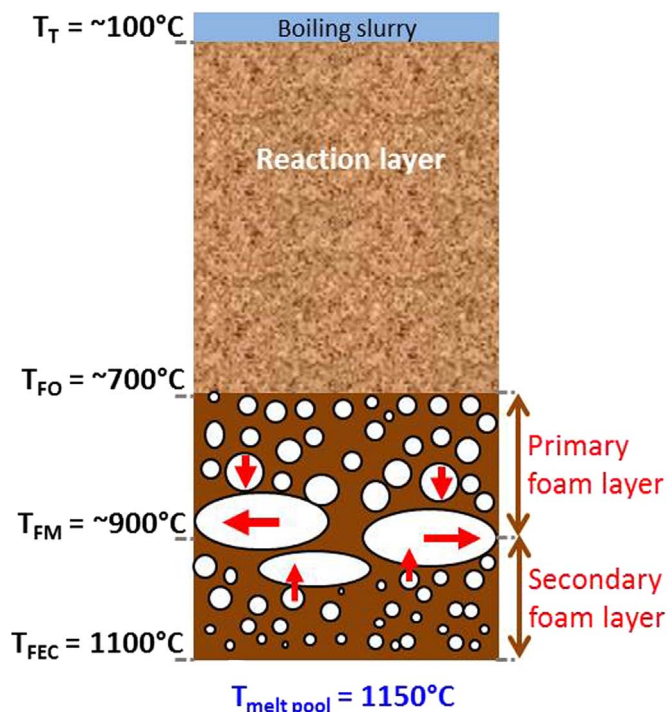


Fig. 1. Schematic of the cold cap (T_T is the cold cap top surface temperature, T_{FO} is the foam onset temperature, T_{FM} is the maximum foam temperature, and T_{FEC} is the effective foam collapse temperature).

In the melter feed, oxidizing components, such as nitrates and nitrites, coexist with reducing components, such as organics. Therefore, O_2 is both produced and consumed throughout the feed-to-glass conversion process. Compositions of the melter feeds are given in Section 2. In Sections 3 and 4, we estimate amounts of O_2 evolved, consumed, and released from melter feeds with different Al_2O_3 sources. Section 5 presents approximation functions that relate O_2 release rate to temperature and time. Then, in Section 6, we use oxygen mass balance to estimate the equilibrium iron redox ratio. Finally, in Section 7, we use the oxygen analyzer data to describe the approach of O_2 partial pressure to equilibrium with the atmosphere.

2. Melter feeds for high-alumina high-level waste (HLW) glass

Table 1 shows the composition of a high-alumina HLW glass and of the associated melter feed containing gibbsite as the alumina source. Feeds with boehmite and corundum mineral sources of alumina were also prepared. These three feeds are simplified versions of melter feeds designed and tested at the Vitreous State Laboratory [23,24]. Feed chemicals were mixed with deionized water to make slurry that was then dried and milled to powder (see [12,29] for details). The chemicals marked red in Table 1 evolve O_2 and the one marked blue consumes it.

3. Reactions involving O_2 at $T < 650$ °C

Before the glass-forming melt becomes connected, massive amounts of H_2O and CO_2 gases are generated from feed reactions together with small amounts of CO , NO , and NO_2 gases [5,10,28]. As glass-forming melt begins gradually to connect into a continuous viscous phase (above approximately 650 °C, Section 4), residual gases are trapped in closed pores [12,29,30]. As pores expand, the melt turns into foam. When foam starts collapsing, the trapped gases are released while O_2 continues to evolve.

The following O_2 -evolving and O_2 -consuming reactions are irrever-

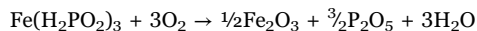
Table 1

Compositions of the glass and feed (to make 1 kg glass).

Glass composition	Mass %	Feed composition	Mass (g)
Al_2O_3	24.16	$Al(OH)_3^{(a)}$	371.79
B_2O_3	19.12	H_3BO_3	341.59
Bi_2O_3	1.16	Bi_2O_3	11.67
CaO	5.74	CaO	10.87
Cr_2O_3	0.52	$Cr_2O_3 \cdot 1.5H_2O$	6.20
F	0.67	NaF	15.00
Fe_2O_3	5.92	$Fe(OH)_3$	74.38
Li_2O	3.59	Li_2CO_3	89.22
Na_2O	9.64	$NaOH$	19.87
NiO	0.40	Na_2CO_3	106.57
P_2O_5	1.06	$NaNO_2$	3.48
PbO	0.41	$NaNO_3$	12.40
SiO_2	27.01	$Na_2C_2O_4$	1.26
SO_3	0.20	$Ni(OH)_2$	5.03
ZrO_2	0.40	PbO	4.17
		SiO_2	221.45
		Na_2SO_4	3.60
		$Zr(OH)_4 \cdot xH_2O$ ($x=0.654$)	5.53
		$Fe(H_2PO_2)_3$	12.51
		$CaSiO_3$ (wollastonite)	97.07
Total	100.00	Total	1413.66

(a) For feeds containing boehmite and corundum, the equivalent masses are 285.94 g and 243.00 g, respectively [10].

sible and complete before glass-forming melt becomes connected:



These reactions are schematic; in reality, oxyanionic salts react with other feed components producing sodium borates, silicates, aluminates, etc. [31]. In the feed of composition listed in Table 1, $NaNO_3$ and $NaNO_2$ would produce 2.334 and 1.571 g O_2 per kg glass, respectively. EGA also detected the formation of small amounts of NO_2 at 380–560 °C. These amounts were equivalent, in g O_2 per kg glass, to 0.028 from the feed with gibbsite, 0.030 from the feed with boehmite, and 0.032 from the feed with corundum. Hence, the actual O_2 release from $NaNO_3$ in the feed with gibbsite, per kg glass, was 2.306 g.

The O_2 -consuming chemicals in the feed (Table 1) are oxalate and hypophosphate. The oxalate could either react with nitrate or decompose, producing CO . The latter reaction would produce 0.268 g CO per kg glass. EGA data showed that 0.246 g CO per kg glass was released at 550 °C. The hypophosphate consumed 4.792 g O_2 per kg glass, which exceeds the O_2 from oxyanionic salts. This explains why no O_2 was detected at temperatures below 650 °C from feeds containing boehmite and corundum. The small amount of O_2 liberated from the feed with gibbsite below 750 °C could possibly originate from Fe_2O_3 (neglecting the minute amount of O_2 from another multivalent oxide, CrO_3), see Section 6. As shown in Section 4, most of the O_2 was released into the atmosphere at temperatures above 850 °C.

4. Reactions involving O_2 at $T > 650$ °C

The release rate of gases from the feeds was measured using the EGA, a gas chromatograph with mass spectrometric detector (Agilent 6890N/5973N) connected to a silica glass tube in the furnace. Feed samples of ~ 1 g were heated to 1150 °C at 10 K min^{-1} under He flowing at 50 ml min^{-1} . The temperature was then held constant at 1150 °C for about 13 min.

Note that an EGA sample represents a tiny amount of melter feed as it moves through the cold cap (Fig. 1) from top to bottom. The heating

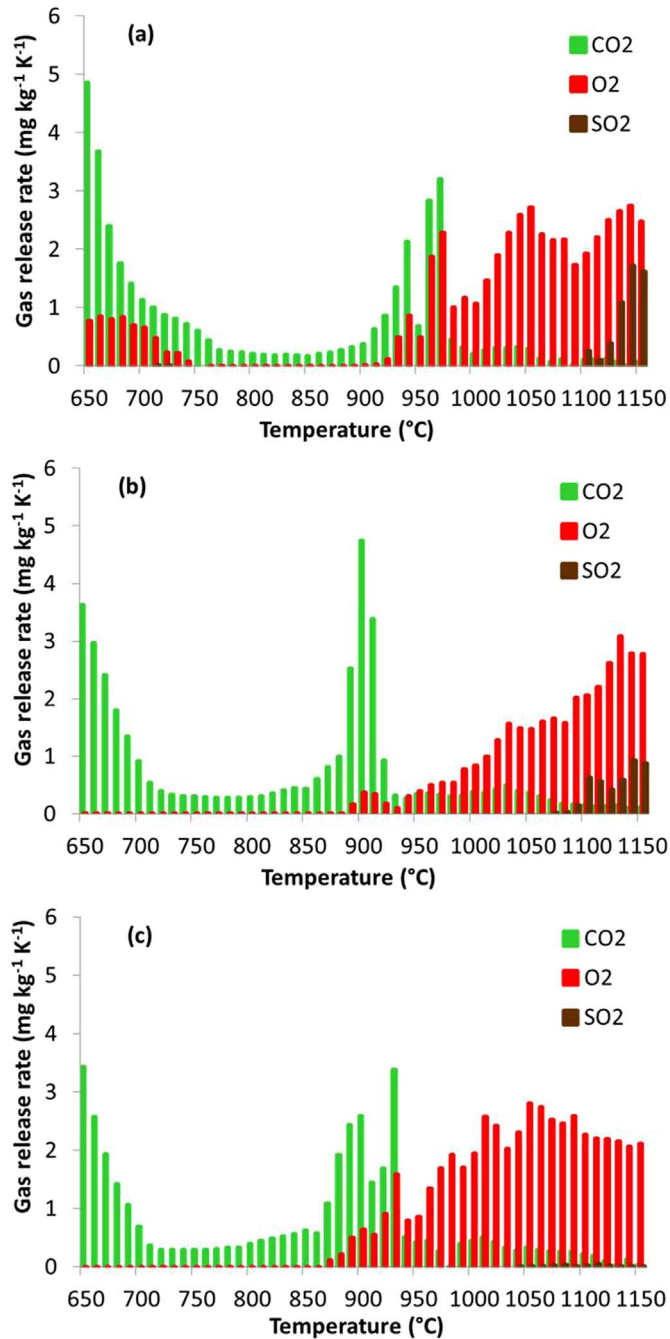


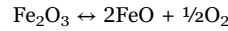
Fig. 2. Gas evolution rates from feeds with (a) gibbsite, (b) boehmite, and (c) corundum.

rate used in the EGA test (10 K min⁻¹) was close to the average of the heating rate that a feed particle experiences during its passage through the cold cap where it varies in dependence of its changing mass, density, heat conductivity, and conversion enthalpy [32,33].

Fig. 2 displays EGA data starting at 650 °C, just as primary foam began to develop. The plot indicates that the trapped gas was mostly a residue of CO₂ that was eventually (at a temperature around 900 °C) released, as the sharp peaks indicate. As mentioned above, little (Fig. 2a) or no (Fig. 2b and c) O₂ was detected at temperatures lower than 650 °C, but O₂ appeared when the foam was collapsing and its release continued for the duration of experiment.

Parallel with the collapse of primary foam, marked by sharp peaks in the CO₂ release rate, secondary foam was sustained by the continued evolution of O₂ and a minute amount of SO₂. In the melter, O₂ bubbles are supplied from redox reactions and sulfate decomposition that occur

in the melt pool below. As the glass composition (Table 1) indicates, most of the O₂ is produced by the reversible reaction [34–37]



Local equilibria of multivalent components, such as Fe, S, or Cr, are functions of local composition and temperature and all depend on the local value of the partial pressure of O₂ [38–40], which, therefore, determines their mutual interaction [36,41]. As the melt becomes uniform with respect to composition and temperature (when residual solids dissolve and diffusion with convection eliminate concentration gradients), the partial pressure of O₂ continues to equilibrate with the atmosphere (Section 7) by a slow process of O₂ diffusion [42].

Although the 0.2 mass% SO₃ in glass (Table 1) is below the solubility limit [43,44], a small fraction of sulfate decomposed by the reaction [37,45,46]



By EGA of the feed with gibbsite, SO₂ began to evolve at 1100 °C and reached 6.7% of total present in the feed during 13 min at 1150 °C (releases during the constant-temperature interval are not shown in Fig. 2). The corresponding amounts of O₂ released from SO₃ were, in g per kg glass, 0.027 from the feed with gibbsite, 0.028 from the feed with boehmite, and 0.001 from the feed with corundum. Oxygen evolution from Fe₂O₃ is examined in Sections 5 and 6.

5. Approximation functions

Apart from the minute release from sulfate, gaseous O₂ was supplied by Fe₂O₃ dissolved in molten glass. The Fe redox ratio, Fe(II)/Fe(III), increased as long as the temperature increased, and approached equilibrium with the atmosphere when the temperature was held constant at 1150 °C. Fig. 3 displays O₂ release rate data measured with EGA during both increasing temperature (solid data points) and constant temperature (open data points). The lines represent two approximation functions fitted to data. For the increasing-temperature segment,

$$\xi_U = \xi_0 \left\{ 1 + \tanh \left[\frac{(T - T_0)}{T_R} \right] \right\} \quad (1)$$

where ξ is the gas evolution rate, T is the temperature, and ξ_0 , T_0 , and T_R are temperature-independent coefficients; subscript U stands for the increasing-temperature segment. For the constant-temperature segment (the decay curve, which is controlled by O₂ diffusion),

$$\xi_D = \xi_i \exp \left(-\frac{t - \Delta t}{t_R} \right) \quad (2)$$

where t is the time, Δt is defined by the intercept between the approximation functions defined by Eqs. (1) and (2), and ξ_1 and t_R are temperature-independent coefficients; subscript D stands for the constant-temperature segment. Table 2 lists coefficient values of both functions for all three feeds. Coefficients of Eq. (1), except ξ_0 , depend on the alumina source. Coefficients of Eq. (2) do not depend on the alumina source, indicating that the melt was homogeneous and compositionally uniform at 1150 °C.

Integrating the right hand side of Eq. (1) yields the total release of O₂ from Fe₂O₃, Ξ_U , during the increasing-temperature segment:

$$\Xi_U = \xi_0 \left\{ T_2 - T_1 + T_R \ln \left[\frac{\cosh \left(\frac{T_2 - T_0}{T_R} \right)}{\cosh \left(\frac{T_1 - T_0}{T_R} \right)} \right] \right\} \quad (3)$$

where $T_1 = 875$ °C and $T_2 = 1150$ °C are the integration limits. Alternatively, based on measured data, we have $\Xi_U = \sum_{i=1}^n \xi_i \Delta T_i$, where ξ_i is the i th measured value, ΔT_i is the temperature interval between consecutive data points, and n is the number of data points (the data are displayed in Figs. 3 and 4). The results listed in Table 2 show that

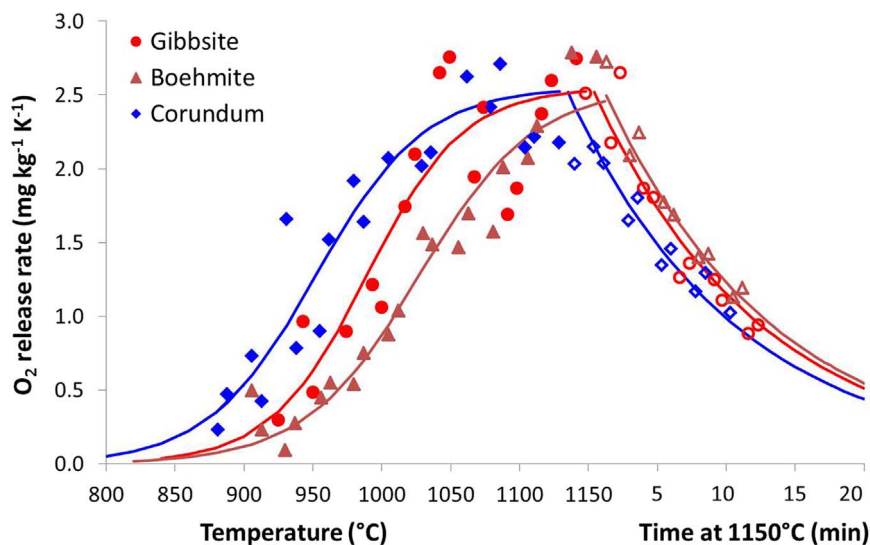


Fig. 3. The rate of O₂ release by EGA.

Table 2

Coefficient values of functions for evolved O₂ gas for the feeds with different alumina sources.

		Gibbsite	Boehmite	Corundum
Increasing temperature (10 K min ⁻¹)				
ξ_0	mg kg ⁻¹ K ⁻¹	1.28	1.28	1.28
T_0	°C	989	1027	952
T_R	K	69.9	83.1	78.3
Ξ_U^a	g kg ⁻¹	0.413	0.336	0.493
Ξ_U^b	g kg ⁻¹	0.415	0.344	0.499
Constant temperature (1150 °C)				
ξ_1	mg kg ⁻¹ min ⁻¹	2.64		
t_R	min	12.28		
Ξ_D	g kg ⁻¹	0.033		

^a integration based on approximation function, Eq. (3).

^b integration based on data.

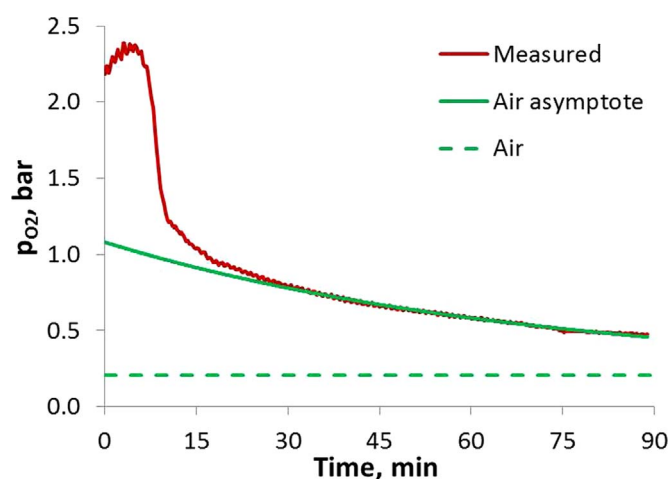


Fig. 4. Partial pressure of oxygen versus time at 1150 °C.

both methods yielded nearly identical values.

Integrating the right hand side of Eq. (2) from $t = 0$ to ∞ , we obtain for the O₂ release, Ξ_D , as Fe redox approaches equilibrium at constant temperature, the formula

$$\Xi_D = \xi_1(t_R - \Delta t) \quad (4)$$

Table 2 lists the resulting values. Because $\Delta t \ll t_R$, the Ξ_D value is virtually same for all three feeds.

Strictly speaking, the numerical coefficients of approximation functions proposed above depend on the glass composition and the heating rate. The glass-forming melt composition changes as the residual solids continue dissolving within the foam layer and even in the melt below the cold cap [47] and, as mentioned in Section 4, the heating rate varies during the passage of melter feed through the cold cap. These are secondary effects that are beyond the scope of this work, but can be taken into account in mathematical models [48].

The effect of alumina source on the O₂ release rate function, $\xi(T)$, is attributable mainly to the effect of the reaction path that the original mineral (gibbsite, boehmite, or corundum) turns into alumina embedded into glass structure [10,27] on foam stability. After gibbsite and boehmite lose the chemically bonded water, they become partly amorphous gels and partly transient aluminoborate minerals [2], whereas corundum persists up to a high temperature (800 °C, [27]).

The main foam stability determining factor in molten glass is the viscosity [49,50]. As is well known, water affects melt viscosity [51]. Gibbsite and boehmite release water at temperatures below 500 °C [5]. This water escapes before it can affect melt viscosity, especially in the EGA test, where the sample is small and the He atmosphere is dry. It is also unlikely that water from feed hydroxides would influence foam stability under the cold cap. Over the decades of viscosity testing of waste glasses, no effect of starting chemicals on melt viscosity was detected.

6. Fe redox

If Fe₂O₃ were fully reduced to FeO, the amount of O₂ produced would be 5.931 g kg⁻¹ glass. The actual amount of O₂ produced from Fe₂O₃ is 5.931z g kg⁻¹, where $z = \text{Fe(II)}/\text{Fe(total)}$ is the fraction reduced, the value of which can be obtained from the oxygen balance:

$$\text{O}_2 \text{ evolved} = \text{O}_2 \text{ consumed} + \text{O}_2 \text{ released}$$

As shown in Sections 2 and 3, O₂ was evolved from nitrates, nitrites, sulfate, and Fe₂O₃, and simultaneously consumed by iron hypophosphate. As shown in Section 5, the amount of O₂ released was $\Xi = \Xi_U + \Xi_D$. Table 3 summarizes the numerical values of O₂ evolved, consumed, and released for feeds with gibbsite, boehmite, and corundum. The O₂ released from Fe₂O₃ was computed using the O₂ balance shown above. Based on this value, the fraction reduced, z , and the redox ratio, $\Gamma = \text{Fe(II)}/\text{Fe(III)}$, were then determined.

Table 3
Summary of values for O₂ mass balance, Fe fraction reduced, and Fe redox ratio.

		Gibbsite	Boehmite	Corundum
O ₂ evolved	g kg ⁻¹ glass	3.904	3.903	3.874
O ₂ consumed	g kg ⁻¹ glass	4.792	4.792	4.792
O ₂ released (EGA)	g kg ⁻¹ glass	0.446	0.369	0.526
O ₂ from Fe ₂ O ₃	g kg ⁻¹ glass	1.334	1.257	1.444
z (Fe fraction reduced)		0.225	0.212	0.243
Γ (Fe redox ratio)		0.290	0.269	0.322

7. Oxygen partial pressure

Oxygen partial pressure, p_{O_2} , determines the redox state of all multivalent species in molten glass [38–40]. The Γ values listed in Table 3 (29% for the feed with gibbsite) are higher than the 2–4% reported for melts equilibrated in air at 1150 °C [52]. The difference is caused by the lower p_{O_2} present in He used as a carrier gas in the EGA equipment ($p_{O_2} = 1.40$ Pa).

The equilibrium constant, K , of the reaction $4Fe^{3+} + 2O^{2-} \rightarrow 4Fe^{2+} + O_2$ is $K = \Gamma^4 p_{O_2}$, where the activity of O^{2-} is included in K . Thus, dropping, for simplicity, the subscript O₂ and using subscripts A and H for air and the He gas used in the EGA equipment, we can write $\Gamma_A = \Gamma_H(p_H/p_A)^{1/4}$. For the feed with gibbsite (Table 3), $\Gamma_H = 0.290$. The p_{O_2} in the He gas was $p_H = 1.40$ Pa. Since $p_A = 2.1 \times 10^4$ Pa, we obtain $\Gamma_A = 0.026$. This value lies between 2% and 4% as expected.

The Fe redox equilibrium is also affected by formation of spinel, typically a solid solution of magnetite (Fe₃O₄), trevorite (NiFe₂O₄), and nichromite (NiCr₂O₄) [53]. For magnetite, $\Gamma = 0.5$ and $z = 0.333$. These values are higher than Γ and z values of glass at equilibrium with He atmosphere at 1150 °C (Table 3). Considering the small content of spinel in glass at 1150 °C (~1%) [48] and the small difference of Fe(II)/Fe(total) in spinel and in the melt [53], we can conclude that spinel formation has a negligible effect on the O₂ balance.

The p_{O_2} in the glass melt was measured with an oxygen analyzer (GS Rapidox II™). About 400 g powder feed containing gibbsite was heated at 10 K min⁻¹ to 1150 °C at which the temperature was held constant for 90 min Fig. 4 displays p_{O_2} versus time elapsed since 1150 °C was reached. After the initial rapid change, the $p_{O_2}(t)$ function was exponential:

$$p = p_\infty - (p_\infty - p_0) \exp\left(-\frac{t}{t_R}\right) \quad (5)$$

where p is the oxygen partial pressure (dropping the subscript O₂) and p_∞ , p_0 , and t_R are constant coefficients. Fitting Eq. (5) to data at $t > 40$ min, while imposing $p_\infty = 0.21$ bar, yielded $p_0 = 1.08$ bar and $t_R = 70.8$ min ($R^2 = 0.993$), indicating that equilibrium with air would be attained at ~5 h.

The chemical analysis of bubbles in quenched samples detected 97.4% O₂ at 1050 °C and 83.6% O₂ at 1150 °C, along with some CO₂, and N₂, and trace amounts of SO₂. The pressure in bubbles in molten glass is ~1 bar considering that hydrostatic pressure and capillary pressure are negligible. With the p_{O_2} values in the melt as high as those shown in Fig. 4, it is not surprising that the oxygen content in bubbles was high.

8. Conclusions

Batch melting reactions that occur in the reaction layer and the primary foam layer of the cold cap, including those producing and consuming O₂, are generally irreversible. Multivalent oxides, such as Fe₂O₃, undergo reversible reactions in molten glass producing O₂, the cumulative amount of which increases as temperature increases. Consequently, the redox reactions play a major role in the formation of secondary foam. The approximation functions defined by Eqs. (1)

and (2) represent O₂ evolution from Fe₂O₃ during both the non-isothermal and isothermal EGA. The EGA in conjunction with stoichiometric calculations allows estimation of both actual and equilibrium redox ratio of the dominant redox constituent (Fe₂O₃) and the associated O₂ partial pressure as functions of temperature.

Acknowledgements

The authors gratefully acknowledge the financial support provided by William F. Hamel, Jr., Federal Project Director, of the U.S. Department of Energy (DOE) Waste Treatment and Immobilization Plant Project. Pacific Northwest National Laboratory is operated by Battelle for DOE under contract DE-AC05-76RL01830. Miroslava Hujová acknowledges financial support from specific university research (MSMT No 20-SVV/2017).

References

- [1] R. Pokorny, A.A. Kruger, P. Hrma, Mathematical modeling of cold cap: effect of bubbling on melting rate, *Ceram. Silik.* 58 (2014) 296–302.
- [2] K. Xu, P. Hrma, J.A. Rice, M.J. Schweiger, B.J. Riley, N.R. Overman, A.A. Kruger, Conversion of nuclear waste to molten glass: cold-cap reactions in crucible test, *J. Am. Ceram. Soc.* 99 (2016) 2964–2970.
- [3] P.A. Smith, J.D. Vienna, P. Hrma, The effects of melting reactions on laboratory-scale waste vitrification, *J. Mater. Res.* 10 (1995) 2137–2149.
- [4] P. Hrma, J. Matyáš, D.-S. Kim. The chemistry and physics of melter cold cap, in: Proceedings of the 9th Biennial Int. Conf. on Nucl. and Hazardous Waste Management, Spectrum '02, American Nuclear Society, CD-ROM, 2002.
- [5] C.P. Rodriguez, J. Chun, M.J. Schweiger, A.A. Kruger, Application of evolved gas analysis to cold-cap reactions of melter feeds for nuclear waste vitrification, *Thermochim. Acta* 592 (2013) 86–92.
- [6] P. Hrma, M.J. Schweiger, C.J. Humrickhouse, J.A. Moody, R.M. Tate, T.T. Rainsdon, N.E. TeGrotenhuis, B.M. Arrigoni, J. Marcial, C.P. Rodriguez, B.H. Tincher, Effect of glass-batch makeup on the melting process, *Ceram. Silik.* 54 (2010) 193–211.
- [7] R. Pokorny, P. Hrma, Mathematical modeling of cold cap, *J. Nucl. Mater.* 429 (2012) 245–256.
- [8] R. Pokorny, D.A. Pierce, P. Hrma, Melting of glass batch: model for multiple overlapping gas-evolving reactions, *Thermochim. Acta* 541 (2012) 8–14.
- [9] J. Chun, D.A. Pierce, R. Pokorny, P. Hrma, Cold-cap reactions in vitrification of nuclear waste glass: experiments and modeling, *Thermochim. Acta* 559 (2013) 32–39.
- [10] S. Lee, P. Hrma, R. Pokorny, J. Klouzek, B.J. VanderVeer, D.R. Dixon, S.A. Luksic, C.P. Rodriguez, J. Chun, M.J. Schweiger, A.A. Kruger, Effect of alumina sources (gibbsite, boehmite, and corundum) on melting behavior of high-level radioactive waste melter feed, in MRS2016, Boston, MA, 2016.
- [11] K.S. Matlack, I.L. Pegg, Advances in JHCM HLW vitrification technology at VSL through scaled melter testing, *Adv. Mater. Sci. Environ. Energy Technol.* II 241 (2013) 47–57.
- [12] S. Lee, B.J. VanderVeer, P. Hrma, Z. Hilliard, J.S. Heilman-Moore, C.C. Bonham, R. Pokorny, D.R. Dixon, M.J. Schweiger, A.A. Kruger, Effects of heating rate, quartz particle size, viscosity, and form of glass additives on high-level waste melter feed volume expansion, *J. Am. Ceram. Soc.* 100 (2017) 583–591.
- [13] M. Cable, Possibilities of progress in glass melting, *J. Non-Cryst. Solids* 73 (1985) 451–461.
- [14] J.A. Bunting, B.H. Bieler, Batch-free time versus crucible volume in glass melting, *Am. Ceram. Soc. Bull.* 48 (1969) 781–785.
- [15] U. Vierneusel, H. Goerk, K.H. Schuller, Suppression of segregation in crucible melts, *Glastech. Ber.* 54 (1981) 332–337.
- [16] M. Cable, Principles of glass melting, in: D.R. Uhlmann, N.J. Kreidl (Eds.), *Glass: Science and Technology*, Academic Press, Orlando, United States, 1984, pp. 1–44.
- [17] F.V. Tooley, Raw materials, *The Handbook of Glass Manufacture* vol. I, Book for Industry, New York, United States, 1974, pp. 19–56.
- [18] R. Beerkens, Analysis of elementary process steps in industrial glass melting tanks—some ideas on innovations in industrial glass melting, *Ceram. Silik.* 52 (2008) 206–217.
- [19] L. Nemeč, Some critical points of the glassmelting process. Part I – dissolution phenomena, *Ceram. Silik.* 39 (1995) 81–86.
- [20] F. Kramer, Gas profile measurements as means of determining gas evolution during glass melting, *Glastech. Ber.* 53 (1980) 177–188.
- [21] D.R. Dixon, D. Cutforth, B. VanderVeer, M.J. Schweiger, P. Hrma, Effect of silica particle size on nuclear waste-to-glass conversion, WM2017 Conference, Phoenix, AZ, March 5–9, 2017.
- [22] D.A. Pierce, P. Hrma, J. Marcial, Thermal analysis of waste glass batches: effect of batch makeup on gas-evolving reactions *Thermal Analysis of Micro, Nano- and Non-crystalline Materials*, Springer, Dordrecht, 2012, pp. 429–440 (Chapter 20).
- [23] K.S. Matlack, H. Gan, M. Chaudhuri, W. Kot, W. Gong, T. Bardakci, I.L. Pegg, I. Joseph, DM100 and DM1200 Melter Testing with High Waste Loading Glass Formulations for Hanford High-Aluminum HLW Streams (VSL-10R-1690-1), Vitreous State Laboratory, Washington, DC, 2010.

- [24] K.S. Matlack, H. Gan, M. Chaudhuri, W. Kot, W. Gong, T. Bardakci, I.L. Pegg, I. Joseph, Melt Rate Enhancement for High Aluminum HLW Glass Formulations (VSL-08R1360-1), Vitreous State Laboratory, Washington, DC, 2008.
- [25] D. Caurant, P. Loiseau, O. Majerus, V. Aubin-Chevaldonnet, I. Bardez, A. Quinta, Glasses, glass-ceramics and ceramics for immobilization of highly radioactive nuclear wastes, in: D. Caurant (Ed.) Glasses, Glass-Ceramics and Ceramics, Nova Science Publishers Inc., New York, United States, 2009, pp. 31–65 (Chapter 3).
- [26] A. Monteiro, S. Schuller, M.J. Toplis, R. Podor, J. Ravau, N. Clavier, H.P. Brau, T. Charpentier, F. Angeli, N. Leterrier, Chemical and mineralogical modifications of simplified radioactive waste calcine during heat treatment, *J. Nucl. Mater.* 448 (2017) 8–19.
- [27] D.A. Pierce, P. Hrma, J. Marcial, B.J. Riley, M.J. Schweiger, Effect of alumina source on the rate of melting demonstrated with nuclear waste glass batch, *Int. J. Appl. Glass Sci.* 3 (2012) 59–68.
- [28] S. Lee, P. Hrma, R. Pokorny, J. Klouzek, B.J. VanderVeer, D.R. Dixon, S.A. Luksic, C.P. Rodriguez, J. Chun, M.J. Schweiger, A.A. Kruger, Effect of melter feed foaming on heat flux to the cold cap, *J. Nucl. Mater.* (2017).
- [29] M.J. Schweiger, P. Hrma, C.J. Humrickhouse, J. Marcial, B.J. Riley, N.E. TeGrotenhuis, Cluster formation of silica particles in glass batches during melting, *J. Non-Cryst. Solids* 356 (2010) 1359–1367.
- [30] W.H. Harris, D.P. Guillen, J. Klouzek, R. Pokorny, T. Yano, S. Lee, M.J. Schweiger, P. Hrma, X-ray tomography of feed-to-glass transition of simulated borosilicate waste glasses, *J. Am. Ceram. Soc.* (2017) 1–12.
- [31] K. Xu, P. Hrma, J. Rice, B.J. Riley, M.J. Schweiger, J.V. Crum, Melter feed reactions at $T \leq 700$ °C for nuclear waste vitrification, *J. Am. Ceram. Soc.* 98 (2015) 3105–3111.
- [32] R. Pokorny, Z.J. Hilliard, D.R. Dixon, M.J. Schweiger, D.P. Guillen, A.A. Kruger, P. Hrma, Cold cap model for melters with bubble, *J. Am. Ceram. Soc.* 98 (2015) 3112–3118.
- [33] D.F. Bickford, P. Hrma, B.W. Bowan II, Control of radioactive waste glass melters: II, Residence time and melt rate limitations, *J. Am. Ceram. Soc.* 73 (1990) 2903–2915.
- [34] A. Paul, R.W. Douglas, Ferrous-ferric equilibrium in binary alkali silicate glasses, *Phys. Chem. Glasses* 6 (1965) 207–211.
- [35] D.S. Goldman, Oxidation equilibrium of iron in borosilicate glass, *J. Am. Ceram. Soc.* 66 (1983) 205–209.
- [36] H.D. Schreiber, A.L. Hockman, Redox chemistry in candidate glasses for nuclear waste immobilization, *J. Am. Ceram. Soc.* 70 (1987) 591–594.
- [37] R. Beerkens, Redox and sulphur reactions in glass melting processes, *Ceram. Silik.* 43 (1999) 123–131.
- [38] R.W. Douglas, P. Nath, A. Paul, Oxygen ion activity and its influence on the redox equilibrium in glasses, *Phys. Chem. Glasses* 6 (1965) 216–223.
- [39] G. Jeddeloh, The redox equilibrium in silicate melts, *Phys. Chem. Glasses* 25 (1984) 163–164.
- [40] P. Hrma, J.D. Vienna, B.K. Wilson, T.J. Plaisted, S.M. Heald, Chromium phase behavior in a multi-component borosilicate glass melt, *J. Non-Cryst. Solids* 352 (2006) 2114–2122.
- [41] A. Paul, R.W. Douglas, Mutual interaction of different redox pairs in glass, *Phys. Chem. Glasses* 7 (1966) 1–13.
- [42] R.G.C. Beerkens, H. de Waal, Mechanism of oxygen diffusion in glassmelts containing variable-valence ions, *J. Am. Ceram. Soc.* 73 (1990) 1857–1861.
- [43] M. Lenoir, A. Grandjean, S. Poissonnet, D.R. Neuville, Quantitation of sulfate solubility in borosilicate glasses using Raman spectroscopy, *J. Non-Cryst. Solids* 355 (2009) 1468–1473.
- [44] J.D. Vienna, D.-S. Kim, I.S. Muller, G.F. Piepel, A.A. Kruger, Toward understanding the effect of low-activity waste glass composition on sulfur solubility, *J. Am. Ceram. Soc.* 97 (2014) 3135–3142.
- [45] J. Klouzek, M. Arkosiova, L. Nemeč, P. Cincibusova, The role of sulphur compounds in glass melting, *J. Glass Sci. Technol.* 48 (2007) 176–182.
- [46] D. Manara, A. Grandjean, O. Pinet, J.L. Dussossoy, D.R. Neuville, Sulfur behavior in silicate glasses and melts: implications for sulfate incorporation in nuclear waste glasses as a function of alkali cation and V_2O_5 content, *J. Non-Cryst. Solids* 353 (2007) 12–23.
- [47] D.R. Dixon, M.J. Schweiger, P. Hrma, Effect of Feeding Rate on the Cold Cap Configuration in a LSM, in WM2013, Phoenix, AZ, 2013 (ISBN 978-0-9836186-2-1).
- [48] R. Pokorny, J.A. Rice, J.V. Crum, M.J. Schweiger, P. Hrma, Kinetic model for quartz and spinel dissolution during melting of high-level-waste glass batch, *J. Nucl. Mater.* 443 (2013) 230–235.
- [49] P. Hrma, Model for a steady state foam blanket, *J. Colloid Interface Sci.* 134 (1990) 161–168.
- [50] J. Marcial, J. Chun, P. Hrma, M.J. Schweiger, Effect of bubbles and silica dissolution on melter feed rheology during conversion to glass, *Environ. Sci. Technol.* 48 (2014) 12173–12180.
- [51] H. Scholze, *Glass, Nature, Structure, and Properties*, Springer, New York, 1990, pp. 171–172.
- [52] P. Hrma, G.F. Piepel, M.J. Schweiger, D.E. Smith, D.-S. Kim, P.E. Redgate, J.D. Vienna, C.A. LoPresti, D.B. Simpson, D.K. Peeler, M.H. Langowski, Property/Composition Relationships for Hanford High-Level Waste Glasses Melting at 1150 °C, Pacific Northwest National Laboratory, Richland, WA, 1994 (PNL-10359).
- [53] P. Hrma, B.J. Riley, J.V. Crum, J. Matyas, The effect of high-level waste glass composition on spinel liquidus temperature, *J. Non-Cryst. Solids* 384 (2014) 32–40.